Newly observed $\Upsilon(10753)$ as a tetraquark state in a chiral quark model with scalar nonet exchange

Yue Tan[‡]
Department of Physics, Yancheng Institute of Technology, Yancheng 224000, People's Republic of China

Xuejie Liu[†]
School of Physics, Southeast University, Nanjing 210094, People's Republic of China

Xiaoyun Chen[§]
College of Science, Jinling Institute of Technology, Nanjing 211169, People's Republic of China

Hongxia Huang[‖] and Jialun Ping[*]
Department of Physics, Nanjing Normal University, Nanjing 210023, People's Republic of China

(Received 1 November 2022; accepted 22 June 2023; published 17 July 2023)

This study investigates the resonance $\omega\chi_{bJ}$, recently discovered in e^+e^- collisions with a center-of-mass energy of $\sqrt{s} = 10.745$ GeV and reported by the Belle II Collaboration, to explore its potential identification with the previously reported $\Upsilon(10753)$. We consider both the traditional $\Upsilon(nS)$ meson and the exotic tetraquark $b\bar{q}q\bar{b}$ state with $J^P = 1^-$, employing the chiral quark model to solve the Schrödinger equation. Our calculations demonstrate that the mass of $\Upsilon(5S)$, $\Upsilon(4S)$, and $\Upsilon(3D)$, as potential two-quark state candidates, are inconsistent with the experimentally observed $\Upsilon(10753)$, effectively excluding the possibility of $\Upsilon(10753)$ as a two-quark state in our model. Furthermore, we employ the Gaussian expansion method to investigate the tetraquark structure of the resonance, including two molecular structures ($b\bar{b}$-$q\bar{q}$, $b\bar{q}$-$q\bar{b}$) and a diquark-antidiquark structure ($\bar{b}\,\bar{q}$-qb), and perform a full-channel coupling using the real-scaling method. Our investigation yields a total of seven resonant states, with one state having an energy of 10761 ± 7 MeV and a width of 10.8 ± 5.2 MeV, which is a promising candidate for the experimentally observed $\Upsilon(10753)$. Furthermore, we report no resonances in the energy range below 10.6 GeV, while several resonances were found in the 10.8–10.9 GeV range. These findings suggest the need for future experiments to search for additional resonant states in this energy range, potentially providing further support for our model.

DOI: 10.1103/PhysRevD.108.014017

I. INTRODUCTION

The discovery of exotic hadrons containing heavy quark pairs, such as the $X(3872)$ reported by the Belle Collaboration in 2003 [1], has opened up a new frontier in the study of hadron spectroscopy. Since then, numerous experiments, including LHCb, ATLAS, CMS, BESIII, Belle, *BABAR*, CDF, and D0, have reported the observation of more than 20 exotic state candidates containing $c\bar{c}$ and $b\bar{b}$ quark pairs (see Fig. 1). These exotic hadrons challenge the conventional picture of mesons as simple $q\bar{q}$ bound states, and their properties offer new insights into the nature of strong interactions beyond the framework of quantum chromodynamics.

The observation of a new structure in the $\chi_{b1}\omega$ invariant mass spectrum by the Belle II Collaboration [2] has recently drawn significant attention. This structure was observed with a significance of 11σ and may correspond to a new state denoted as $\Upsilon(10753)$. The Belle II Collaboration combined their data with previous Belle results at $\sqrt{s} = 10.867$ GeV and found energy dependencies of the Born cross sections for $e^+e^- \to \omega\chi_{b1,b2}(1P)$ consistent with the shape of the newly observed state. Furthermore, the decay mode $\chi_{bJ}\omega$ of $\Upsilon(10753)$ suggests

[*]Corresponding author.
jlping@njnu.edu.cn
[†]Corresponding author.
101300036@seu.edu
[‡]tanyue@ycit.edu.cn
[§]xychen@jit.edu.cn
[‖]HongxiaHuang@njnu.edu.cn

that it may consist of a $b\bar{b}$ quark pair and a $q\bar{q}$ quark pair. Since its mass is above the threshold of $\chi_{bJ}\omega$, the possible candidates of $\Upsilon(10753)$ are colorful subclusters $bq\text{-}\bar{q}\,\bar{b}$ or radial excited $b\bar{b}$. The Belle Collaboration has also suggested that the quantum numbers of the state are $J^P = 1^-$. This discovery provides further evidence of the existence of exotic hadrons and opens up new avenues for the study of low-energy QCD.

$$M_{\Upsilon(10753)} = 10753 \pm 6.0 \text{ MeV}$$
$$\Gamma_{\Upsilon(10753)} = 36^{+18}_{-12} \text{ MeV}$$

The heavy quarkonium system exhibits significant differences between the charmonium and bottomium systems with respect to exotic states. While only two exotic candidates, $Z_b(10610)$ and $Z_b(10650)$, have been reported in the bottomium system by the Belle Collaboration [3,4], the charmonium system has a larger abundance of exotic states due to the lower threshold, DD, which is less than almost half of the $c\bar{c}$ states. However, the recent observation of a new structure in the $\chi_{b1}\omega$ invariant mass spectrum by the Belle II Collaboration may change this trend. This new structure, possibly identified as $\Upsilon(10753)$, not only enriches the bottomium family but also raises our interest in the negative parity $b\bar{b}q\bar{q}$ system. Prior to this observation, there has been a significant amount of research on the negative parity $b\bar{b}q\bar{q}$ system, with interpretations ranging from traditional bottomonium, tetraquark state, to hybrid. For example, Ref. [5] interpreted $\Upsilon(10753)$ as a 3^3D_1 $b\bar{b}$ state using relativistic flux tube model with spin-dependent interactions, while Ref. [6] interpreted it as a S-D mixing state dominated by the D-wave component. However, it is still unclear what mechanism causes such a significant mixing between $\Upsilon(5S)$ and $\Upsilon(4D)$. Due to the large mass of the b quark compared to the other quarks, the tensor-force and spin-orbit matrix element are relatively small, which may reduce the coupling effect between the S- and D-wave components. Some researchers suggest that the diquark-antidiquark tetraquark state may be responsible for the existence of $\Upsilon(10753)$. For instance, Ref. [7] assigned $\Upsilon(10753)$ as the diquark-antidiquark-type vector hidden-bottom tetraquark state by QCD sum rules. In Ref. [8], the authors investigated $\Upsilon(10753)$ by considering the quarkonium and meson-meson components of $\Upsilon(nS)$, including $\Upsilon(10860)$, and confirmed that $\Upsilon(10753)$ may have 76% meson-meson content. In Ref. [9], the author treated $\Upsilon(10753)$ as a linear combination of the diquark-antidiquark and $b\bar{b}$ components due to the mixing via gluonic exchanges.

In recent years, there has been increasing interest in the possibility that the $\Upsilon(10753)$ may be a compact tetraquark made up of a $bq\text{-}\bar{q}\,\bar{b}$ substructure. If this is the case, the interaction between the two subclusters may be influenced by an isoscalar $q\bar{q}$ pair. However, one long-standing problem with quark models is the ρ-ω mass reversal, which arises from the lack of an isospin-dependent mechanism in the light-quark sector [10,11]. One approach to addressing this issue is to add extra scalar meson exchanges to the Goldstone boson exchange, as done in Ref. [12]. However, this approach requires several parameters to replace the scalar-meson exchange. In this study, we propose a framework based on $SU(3)$ symmetry that incorporates scalar nonet exchange in a chiral quark model, with the aim of better describing the isoscalar $b\bar{q}q\bar{b}$ system without requiring additional parameters. To calculate the tetraquark properties, we use the Rayleigh-Ritz variational method with a Gaussian expansion method (GEM), which allows us to expand each relative motion in the system in terms of Gaussian basis functions. We also consider the mixing effect of molecular and diquark-antidiquark structures. While it is theoretically possible to describe the system with a sufficient number of excited bases, it is not practical to include too many bases in our calculation. To address this issue, we combine different structures and keep the subclusters in low-lying states. However, combining different structures can lead to overcalculation, so we remove strange bases in the Hamiltonian matrix with an eigenvalue of zero and reintegrate the remaining bases into a new Hamiltonian matrix. Finally, we use the real-scaling method to confirm the presence of bound states and genuine resonances, and to obtain their decay widths.

The paper is organized as follows. After the introduction, details of ChQM and GEM are introduced in Sec. II. In Sec. III, we present the numerical results and a method of finding and calculating the decay width of the genuine resonance state. The last section is devoted to the summary.

II. CHIRAL QUARK MODEL, WAVE FUNCTION OF $b\bar{q}q\bar{b}$ SYSTEM

A. Chiral quark model

The chiral quark model has been applied successfully in describing the hadron spectra and hadron-hadron interactions. The details of the model can be found in Refs. [11,13,14]. In this writing, we introduce a chiral quark model with scalar nonet exchange. The Hamiltonian of the chiral quark model is given as follows:

$$H = \sum_{i=1}^{n} m_i + \sum_{i=1}^{n}\left(\frac{p_i^2}{2m_i} - T_{CM}\right) + \sum_{i<j=1}^{n}\Bigg[V_{\text{con}}(r_{ij}) + V_{\text{oge}}(r_{ij}) + \sum_{\chi=\pi,\eta,K} V_\chi(r_{ij}) + \sum_{s=a_0,f_0,\kappa} V_s(r_{ij})\Bigg], \quad (1)$$

where m_i is the constituent mass of ith quark (antiquark), and μ is the reduced masse of two interacting quarks or quark clusters. T_{CM} is the kinetic energy of the center-of-mass motion. For the two-quark structure, the kinetic-energy term $\sum_{i=1}^{n}(\frac{p_i^2}{2m_i} - T_{CM})$ will degenerate into $\frac{p_{12}^2}{2\mu_{12}}$,

while the kinetic-energy term of tetraquark system can be written as $\frac{p_{12}^2}{2\mu_{12}}+\frac{p_{34}^2}{2\mu_{34}}+\frac{p_{12,34}^2}{2\mu_{12,34}}$, where

$$\mu_{ij}=\frac{m_i m_j}{m_i+m_j}, \qquad ij=12,34 \tag{2}$$

$$\mu_{1234}=\frac{(m_1+m_2)(m_3+m_4)}{m_1+m_2+m_3+m_4}, \tag{3}$$

$$p_{ij}=\frac{m_j p_i-m_i p_j}{m_i+m_j}, \tag{4}$$

$$p_{1234}=\frac{(m_3+m_4)p_{12}-(m_1+m_2)p_{34}}{m_1+m_2+m_3+m_4}. \tag{5}$$

The different terms of the potential contain central, spin-orbit contributions and tensor force. However, it is difficult for us to deal with spin-orbit and tensor force contributions when it comes to the computation of four quarks. Thus, spin-orbit coupling, tensor force, and central force contributes to our two-quark calculation while only central force contributes to our four-quark calculation.

$V_{\rm con}(r_{ij})$ is the confining potential, mimics the "confinement" property of QCD. The $V_{\rm con}(r_{ij})$ term includes central force $V_{\rm con}^{C}(r_{ij})$ and spin-orbit force $V_{\rm con}^{\rm SO}(r_{ij})$,

$$\begin{cases} V_{\rm con}^{C}(r_{ij})=(-a_c r_{ij}^2-\Delta)\boldsymbol{\lambda}_i^c\cdot\boldsymbol{\lambda}_j^c \\ V_{\rm con}^{\rm SO}(r_{ij})=-\boldsymbol{\lambda}_i^c\cdot\boldsymbol{\lambda}_j^c\frac{a_c}{4m_i^2m_j^2}[((m_i^2+m_j^2)(1-2a_s) \\ +4m_i m_j(1-a_s))(\vec{S}_+\cdot\vec{L}) \\ +((m_j^2-m_i^2)(1-2a_s))(\vec{S}_-\cdot\vec{L})]. \end{cases} \tag{6}$$

The second potential $V_{\rm oge}(r_{ij})$ is a one-gluon exchange interaction reflecting the "asymptotic freedom" property of QCD. The $V_{\rm oge}(r_{ij})$ term contains central force $V_{\rm oge}^{C}(r_{ij})$, spin-orbit force $V_{\rm oge}^{\rm SO}(r_{ij})$, and tensor force $V_{\rm oge}^{T}(r_{ij})$,

$$\begin{cases} V_{\rm oge}^{C}(r_{ij})=\frac{\alpha_s}{4}\boldsymbol{\lambda}_i^c\cdot\boldsymbol{\lambda}_j^c\left[\frac{1}{r_{ij}}-\frac{1}{6m_i m_j r_0^2}\boldsymbol{\sigma}_i\cdot\boldsymbol{\sigma}_j\frac{e^{-r_{ij}/r_0(\mu_{ij})}}{r_{ij}}\right] \\ V_{\rm oge}^{\rm SO}(r_{ij})=-\frac{1}{16}\frac{\alpha_s\boldsymbol{\lambda}_i^c\cdot\boldsymbol{\lambda}_j^c}{4m_i^2m_j^2}\left[\frac{1}{r_{ij}^3}-\frac{e^{-r_{ij}/r_g(\mu)}}{r_{ij}^3}\left(1+\frac{r_{ij}}{r_g(\mu)}\right)\right] \\ [(m_i^2+m_j^2+4m_i m_j)(\vec{S}_+\cdot\vec{L})+(m_j^2-m_i^2)(\vec{S}_-\cdot\vec{L})] \\ V_{\rm oge}^{T}(r_{ij})=-\frac{1}{16}\frac{\alpha_s\boldsymbol{\lambda}_i^c\cdot\boldsymbol{\lambda}_j^c}{4m_i^2m_j^2}\left[\frac{1}{r_{ij}^3}-\frac{e^{-r_{ij}/r_g(\mu)}}{r_{ij}}\left(\frac{1}{r_{ij}^2}\right.\right. \\ \left.\left.+\frac{1}{3r_g^2(\mu)}+\frac{1}{r_{ij}r_g(\mu)}\right)\right]S_{ij}, \end{cases} \tag{7}$$

where $\boldsymbol{\sigma}$ are the $SU(2)$ Pauli matrices; $\boldsymbol{\lambda}_c$ are the $SU(3)$ color Gell-Mann matrices, $r_0(\mu_{ij})=\frac{r_0}{\mu_{ij}}$ and α_s is an effective scale-dependent running coupling,

$$\alpha_s(\mu_{ij})=\frac{\alpha_0}{\ln[(\mu_{ij}^2+\mu_0^2)/\Lambda_0^2]}. \tag{8}$$

The third potential $V_{\chi,s}$ is Goldstone boson exchange, coming from "chiral symmetry spontaneous breaking" of QCD in the low-energy region. There are two different contributions including pseudoscalar-meson exchange $V_{\chi=\pi,\eta,K}(r_{ij})$ and scalar-meson exchange $V_{s=a_0,f_0,\kappa,\sigma}(r_{ij})$ to the Goldstone boson exchange. The pseudoscalar-meson exchange $V_{\chi=\pi,\eta,K}(r_{ij})$ contains central force and tensor force while the scalar meson exchange $V_{s=a_0,f_0,\kappa,\sigma}(r_{ij})$ consists of central force contribution and spin-orbit contribution,

$$\begin{cases} V_\chi(r_{ij})=v_\pi(\mathbf{r}_{ij})\sum_{a=1}^{3}\lambda_i^a\lambda_j^a+v_K(\mathbf{r}_{ij})\sum_{a=4}^{7}\lambda_i^a\lambda_j^a \\ +v_\eta(\mathbf{r}_{ij})\left[\cos\theta_P(\lambda_i^8\lambda_j^8)-\sin\theta_P(\lambda_i^0\lambda_j^0)\right], \\ v_{\chi=\pi,K,\eta}^{C}=\frac{g_{\rm ch}^2}{4\pi}\frac{m_\chi^2}{\Lambda_\chi^2-m_\chi^2}\frac{\Lambda_\chi^2}{\Lambda_\chi^2-m_\chi^2}m_\chi\left[Y(m_\chi r_{ij})\right. \\ \left.-\frac{\Lambda_\chi^3}{m_\chi^3}Y(\Lambda_\chi r_{ij})\right](\vec{\sigma}_i\cdot\vec{\sigma}_j), \\ v_{\chi=\pi,K,\eta}^{T}=\frac{g_{\rm ch}^2}{4\pi}\frac{m_\chi^2}{\Lambda_\chi^2-m_\chi^2}\frac{\Lambda_\chi^2}{\Lambda_\chi^2-m_\chi^2}m_\chi\left[H(m_\chi r_{ij})\right. \\ \left.-\frac{\Lambda_\chi^3}{m_\chi^3}H(\Lambda_\chi r_{ij})\right]S_{ij}, \end{cases} \tag{9}$$

$$\begin{cases} V_S(r_{ij})=v_\sigma(\mathbf{r}_{ij})\lambda_i^0\lambda_j^0+v_{a_0}(\mathbf{r}_{ij})\sum_{a=1}^{3}\lambda_i^a\lambda_j^a \\ +v_\kappa(\mathbf{r}_{ij})\sum_{a=4}^{7}\lambda_i^a\lambda_j^a+v_{f_0}(\mathbf{r}_{ij})\lambda_i^8\lambda_j^8 \\ v_{s=\sigma,a_0,f_0,\kappa}^{C}=-\frac{g_{\rm ch}^2}{4\pi}\frac{\Lambda_s^2}{\Lambda_s^2-m_s^2}m_s\left[Y(m_s r_{ij})-\frac{\Lambda_s}{m_s}Y(\Lambda_s r_{ij})\right], \\ v_{s=\sigma,a_0,f_0,\kappa}^{\rm SO}=-\frac{g_{\rm ch}^2}{4\pi}\frac{\Lambda_s^2}{\Lambda_s^2-m_s^2}\frac{m_s^3}{2m_i m_j}\left[G(m_s r_{ij})\right. \\ \left.-\frac{\Lambda_s^3}{m_s^3}G(\Lambda_s r_{ij})\right]\vec{L}\cdot\vec{S}, \end{cases} \tag{10}$$

$\boldsymbol{\lambda}$ are $SU(3)$ flavor Gell-Mann matrices, $m_{\chi(s)}$ are the masses of Goldstone bosons, $\Lambda_{\chi(s)}$ are the cutoffs, $g_{\rm ch}^2/4\pi$ is the Goldstone-quark coupling constant. The quark-tensor operator is determined by $S_{ij}=3(\vec{\sigma}_i\cdot\hat{r}_{ij})(\vec{\sigma}_j\cdot\hat{r}_{ij})-(\vec{\sigma}_i\cdot\vec{\sigma}_j)$. Finally, $Y(x)$ is the standard Yukawa function defined by $Y(x)=e^{-x}/x$, $G(x)=(1+1/x)Y(x)/x$ and $H(x)=(1+3/x+3/x^2)Y(x)/x$.

All the parameters are determined by fitting the meson spectrum, from light mesons (π, η) to heavy mesons (χ_{bJ}), taking into account only a quark-antiquark component. They are shown in Table I. The calculated masses of the mesons involved in the present work are shown in Table II.

TABLE I. Quark model parameters ($m_\pi = 0.7$ fm^{-1}, $m_\sigma = 3.42$ fm^{-1}, $m_\eta = 2.77$ fm^{-1}). There are two sets of chiral quark model parameters, the different parts of which are separated by "/".

Quark masses	$m_u = m_d$(MeV)	490/499
	m_b(MeV)	4978/4980
Goldstone bosons	Λ_π(fm^{-1})	3.5
	Λ_η(fm^{-1})	2.2
	Λ_{a0}(fm^{-1})	2.5
	Λ_{f0}(fm^{-1})	1.2
	$g^2_{\rm ch}/(4\pi)$	0.54
	θ_p(°)	−15
Confinement	a_c(MeV)	98
	Δ(MeV)	−18.1
OGE	α_{qq}	1.34/1.35
	α_{qb}	0.75/0.76
	α_{bb}	0.43/0.44
	$\hat{r}_0$(MeV)	81.0
	$\hat{r}_g$(MeV)	100.6
	a_s	0.77

B. The wave function of $b\bar{q}q\bar{b}$ system

There are two physically important structures, meson-meson, and diquark-antidiquark in the $b\bar{b}q\bar{q}$ system, which are considered in the present calculation. The wave functions of every structure all consists of four parts: orbital, spin, flavor, and color. The wave function of each part is constructed in two steps; first write down the two-body wave functions, then couple two subclusters wave functions to form the four-body one. To distinguish different structures, we give every quark with specific particle order (b_1, $\bar{q}_2$, q_3, $\bar{b}_4$). As a consequence, the b_1 coupled with $\bar{q}_2$ while the q_3 coupled with $\bar{b}_4$ can lead to the dimeson $b_1\bar{q}_2$-$q_3\bar{b}_4$ structure. If we couple the $b_1\bar{b}_3$ into the first subcluster and $q_2\bar{q}_4$ into the second subcluster, the $b_1\bar{b}_4$-$q_3\bar{q}_2$-type dimeson states can be obtained. As for the diquark-antidiquark structure, its particle order is b_1q_3-$\bar{q}_2\bar{b}_4$. All of the three structures can be found in Fig. 2. In this treatment, its convenient for us to do coupling calculation between different structures. With the certain isospin, three kinds of flavor wave functions are obtained in Eq. (11). Considering that the difference of each structure is particle order, we only present the spatial wave function, spin wave function, and color wave function of the $b_1\bar{q}_2$-$q_3\bar{b}_4$ dimeson structure and the other color wave-function of the b_1q_3-q_2b_4 diquark-antidiquark structure in the next subsection for simplicity. However, we should keep in mind, when we deal with the other structures, the particles order should be adjusted correctly. Because there are no identical particles in the system, the total wave function of the system is the direct product of spatial ($|R_i\rangle$), spin ($|S_j\rangle$), color ($|C_k\rangle$), and flavor ($|F_n\rangle$) wave functions with necessary coupling.

TABLE II. Numerical results for the meson spectrum (in MeV) for the ChQM1(with a harmonic-form confinement), the ChQM2 (with a color screening-form confinement) and relative quark model. (unit: MeV).

Meson	Para.1	Para.2	ChQM2[12]	RM[15]	EXP.(PDG)
π	149	141	139	···	139.57 ± 0.00035
η	524	582	572	···	547.862 ± 0.017
ρ	765	768	775	···	775.26 ± 0.34
ω	780	784	691	···	782.66 ± 0.13
B	5273	5277	5281	···	5279.66 ± 0.12
B^*	5329	5355	5321	···	5324.71 ± 0.21
B_0	5770	5774	···	···	···
B_1	5813	5817	···	···	$5725.9^{+2.5}_{-2.7}$
B_2	5850	5855	5790	···	5735.2 ± 0.7
η_b	9390	9365	9454	9390	9398.7 ± 2.0
$\Upsilon(1S)$	9499	9484	9505	9460	9460.3 ± 0.26
$\Upsilon(2S)$	9968	9964	10013	10015	10023.6 ± 0.31
$\Upsilon(3S)$	10278	10276	10335	10343	10355.2 ± 0.5
$\Upsilon(4S)$	10564	10563	10577	10579	10579.4 ± 1.2
$\Upsilon(3D)$	10631	10644	···	···	10579.4 ± 1.2
$\Upsilon(5S)$	10863	10862	10770	10811	$10885.2^{+2.6}_{-1.6}$
h_b	9897	9895	···	9909	9899.3 ± 0.8
χ_{b0}	9865	9861	9855	9864	$9859.44 \pm 0.42 \pm 0.31$
χ_{b1}	9891	9888	9875	9903	$9892.78 \pm 0.26 \pm 0.31$
χ_{b2}	9908	9907	9887	9921	$9912.21 \pm 0.26 \pm 0.31$

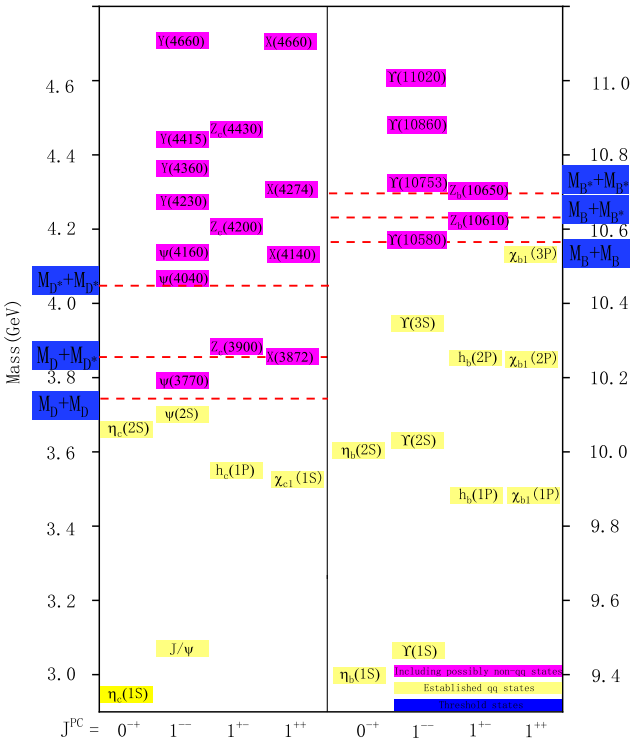

FIG. 1. Energy spectrum of $c\bar{c}$ and $b\bar{b}$ system.

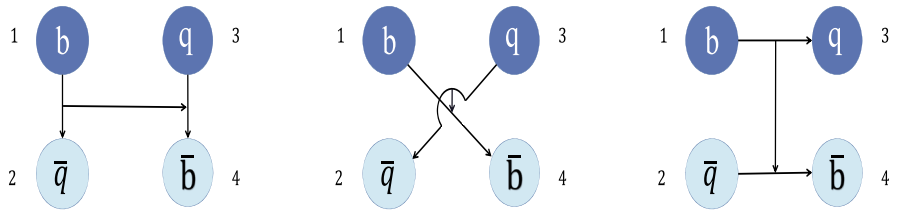

FIG. 2. Three kinds of configuration of b, $\bar{b}$, q, and $\bar{q}$ system: (a) the molecular configuration of $bq\bar{q}\,\bar{b}$ system; (b) the molecular configurations of $bb\bar{q}\,\bar{q}$ system; (c) the diquark-antidiquark configurations of $bq\bar{b}\,\bar{q}$ system.

1. Flavor wave function

We have three flavor wave functions of the system,

$$|F_1\rangle = \frac{1}{\sqrt{2}}(b_1\bar{u}_2u_3\bar{b}_4 + b_1\bar{d}_2d_3\bar{b}_4), \tag{11}$$

$$|F_2\rangle = \frac{1}{\sqrt{2}}(b_1\bar{b}_4u_3\bar{u}_2 + b_1\bar{b}_4d_3\bar{d}_2), \tag{12}$$

$$|F_3\rangle = \frac{1}{\sqrt{2}}(b_1u_3\bar{u}_2\bar{b}_4 + b_1d_3\bar{d}_2\bar{b}_4), \tag{13}$$

$|F_1\rangle$, $|F_2\rangle$ is for meson-meson structure, and $|F_3\rangle$ is for diquark-antidiquark structure.

2. Spatial wave function

The orbital wave function of the four-quark system consists of two subcluster orbital wave function and the relative motion wave function between two subclusters,

$$\begin{aligned}
|R_1\rangle &= [[\Psi_{l_1=1}(\mathbf{r}_{12})\Psi_{l_2=0}(\mathbf{r}_{34})]_{l_{12}}\Psi_{L_r}(\mathbf{r}_{1234})]^{M_L}_L,\\
|R_2\rangle &= [[\Psi_{l_1=0}(\mathbf{r}_{14})\Psi_{l_2=1}(\mathbf{r}_{32})]_{l_{12}}\Psi_{L_r}(\mathbf{r}_{1432})]^{M_L}_L,\\
|R_3\rangle &= [[\Psi_{l_1=1}(\mathbf{r}_{13})\Psi_{l_2=0}(\mathbf{r}_{24})]_{l_{12}}\Psi_{L_r}(\mathbf{r}_{1432})]^{M_L}_L,
\end{aligned} \tag{14}$$

where the bracket "[ ]" indicates orbital angular momentum coupling, and L is the total orbital angular momentum which comes from the coupling of L_r (orbital angular momentum of relative motion) and l_{12} which is derived by coupling l_1 and l_2. The l_1 (l_2) is subcluster orbital angular momenta. $|R_{i,i=1,2}\rangle$ are used to represent the orbital wave functions of meson-meson structure, and $|R_{i=3,4}\rangle$ are used to represent the wave functions of diquark-antidiquark structure. In GEM [16], the radial part of the orbital wave function is expanded by a set of Gaussians,

$$\Psi(\mathbf{r}) = \sum_{n=1}^{n_{\max}} c_n\psi^G_{nlm}(\mathbf{r}), \tag{15a}$$

$$\psi^G_{nlm}(\mathbf{r}) = N_{nl}r^l e^{-\nu_n r^2}Y_{lm}(\hat{\mathbf{r}}), \tag{15b}$$

where N_{nl} are normalization constants,

$$N_{nl} = \left[\frac{2^{l+2}(2\nu_n)^{l+\frac{3}{2}}}{\sqrt{\pi}(2l+1)}\right]^{\frac{1}{2}}. \tag{16}$$

c_n are the variational parameters, which are determined dynamically. The Gaussian size parameters are chosen according to the following geometric progression

$$\nu_n = \frac{1}{r_n^2}, \qquad r_n = r_1a^{n-1}, \qquad a = \left(\frac{r_{n_{\max}}}{r_1}\right)^{\frac{1}{n_{\max}-1}}. \tag{17}$$

This procedure enables optimization of the using of Gaussians; as small as possible Gaussians are used.

3. Spin wave function

Because there is no difference between the spin of quarks and antiquarks, the meson-meson structure has the same spin wave function as the diquark-antidiquark structure. The spin wave functions of the subcluster are shown below:

$$\chi^\sigma_{11} = \alpha\alpha, \qquad \chi^\sigma_{10} = \frac{1}{\sqrt{2}}(\alpha\beta + \beta\alpha), \qquad \chi^\sigma_{1-1} = \beta\beta,$$
$$\chi^\sigma_{00} = \frac{1}{\sqrt{2}}(\alpha\beta - \beta\alpha).$$

Coupling the spin wave functions of two subclusters by Clebsch-Gordan coefficients, total spin wave function can be written below,

$$\begin{aligned}
|S_1\rangle = \chi^{\sigma 1}_0 = \sqrt{\frac{1}{4}}(&\alpha_1\beta_2\alpha_3\beta_4 - \alpha_1\beta_2\beta_3\alpha_4 - \beta_1\alpha_2\alpha_3\beta_4\\
&+ \beta_1\alpha_2\beta_3\alpha_4),
\end{aligned} \tag{18}$$

$$\begin{aligned}
|S_2\rangle = \chi^{\sigma 2}_0 = \sqrt{\frac{1}{12}}(&2\alpha_1\alpha_2\beta_3\beta_4 + 2\beta_1\beta_2\alpha_3\alpha_4 - \alpha_1\beta_2\alpha_3\beta_4\\
&- \alpha_1\beta_2\beta_3\alpha_4 - \beta_1\alpha_2\alpha_3\beta_4 - \beta_1\alpha_2\beta_3\alpha_4),
\end{aligned} \tag{19}$$

$$|S_3\rangle = \chi_1^{\sigma 3} = \sqrt{\frac{1}{4}}(\alpha_1\beta_2\alpha_3\beta_4 + \alpha_1\beta_2\beta_3\alpha_4 - \beta_1\alpha_2\alpha_3\beta_4 - \beta_1\alpha_2\beta_3\alpha_4), \tag{20}$$

$$|S_4\rangle = \chi_1^{\sigma 4} = \sqrt{\frac{1}{4}}(\alpha_1\beta_2\alpha_3\beta_4 - \alpha_1\beta_2\beta_3\alpha_4 + \beta_1\alpha_2\alpha_3\beta_4 \tag{21}$$

$$|S_5\rangle = \chi_1^{\sigma 5} = \sqrt{\frac{1}{2}}(\alpha_1\alpha_2\beta_3\beta_4 - \beta_1\beta_2\alpha_3\alpha_4), \tag{22}$$

$$|S_6\rangle = \chi_2^{\sigma 6} = \sqrt{\frac{1}{6}}(\alpha_1\alpha_2\beta_3\beta_4 + \beta_1\beta_2\alpha_3\alpha_4 + \alpha_1\beta_2\alpha_3\beta_4 + \alpha_1\beta_2\beta_3\alpha_4 + \beta_1\alpha_2\alpha_3\beta_4 + \beta_1\alpha_2\beta_3\alpha_4). \tag{23}$$

The total spin wave function is denoted by $\chi_S^{\sigma i}$, i is the index of the functions, the S is the total spin of the system. Due to absence of a spin-dependent interaction in the Hamiltonian which can distinguish the third component of the spin quantum number, we set the third component of the spin to be zero for simplicity.

4. Color wave function

The colorless tetraquark system has four color wave functions, two for meson-meson structure, $1 \otimes 1$ (C_1), $8 \otimes 8$ (C_2), and two for diquark-antidiquark structure, $\bar{3} \otimes 3$ (C_3) and $6 \otimes \bar{6}$ (C_4),

$$|C_1\rangle = \sqrt{\frac{1}{9}}\Big(r_1\bar{r}_2r_3\bar{r}_4 + r_1\bar{r}_2g_3\bar{g}_4 + r_1\bar{r}_2b_3\bar{b}_4 + g_1\bar{g}_2r_3\bar{r}_4 + g_1\bar{g}_2g_3\bar{g}_4 + g_1\bar{g}_2b_3\bar{b}_4 + b_1\bar{b}_2r_3\bar{r}_4 + b_1\bar{b}_2g_3\bar{g}_4 + b_1\bar{b}_2b_3\bar{b}_4\Big),$$

$$|C_2\rangle = \sqrt{\frac{1}{72}}\Big(3r_1\bar{b}_2b_3\bar{r}_4 + 3r_1\bar{g}_2g_3\bar{r}_4 + 3g_1\bar{b}_2b_3\bar{g}_4 + 3b_1\bar{g}_2g_3\bar{b}_4 + 3g_1\bar{r}_2r_3\bar{g}_4 + 3b_1\bar{r}_2r_3\bar{b}_4 + 2r_1\bar{r}_2r_3\bar{r}_4 + 2g_1\bar{g}_2g_3\bar{g}_4 + 2b_1\bar{b}_2b_3\bar{b}_4 - r_1\bar{r}_2g_3\bar{g}_4 - g_1\bar{g}_2r_3\bar{r}_4 - b_1\bar{b}_2g_3\bar{g}_4 - b_1\bar{b}_2r_3\bar{r}_4 - g_1\bar{g}_2b_3\bar{b}_4 - r_1\bar{r}_2b_3\bar{b}_4\Big),$$

$$|C_3\rangle = \sqrt{\frac{1}{12}}\Big(r_1g_3\bar{r}_2\bar{g}_4 - r_1g_3\bar{g}_2\bar{r}_4 + g_1r_3\bar{g}_2\bar{r}_4 - g_1r_3\bar{r}_2\bar{g}_4 + r_1b_3\bar{r}_2\bar{b}_4 - r_1b_3\bar{b}_2\bar{r}_4 + b_1r_3\bar{b}_2\bar{r}_4 - b_1r_3\bar{r}_2\bar{b}_4 + g_1b_3\bar{g}_2\bar{b}_4 - g_1b_3\bar{b}_2\bar{g}_4 + b_1g_3\bar{b}_2\bar{g}_4 - b_1g_3\bar{g}_2\bar{b}_4\Big),$$

$$|C_4\rangle = \sqrt{\frac{1}{24}}\Big(2r_1r_3\bar{r}_2\bar{r}_4 + 2g_1g_3\bar{g}_2\bar{g}_4 + 2b_1b_3\bar{b}_2\bar{b}_4 + r_1g_3\bar{r}_2\bar{g}_4 + r_1g_3\bar{g}_2\bar{r}_4 + g_1r_3\bar{g}_2\bar{r}_4 + g_1r_3\bar{r}_2\bar{g}_4 + r_1b_3\bar{r}_2\bar{b}_4 + r_1b_3\bar{b}_2\bar{r}_4 + b_1r_3\bar{b}_2\bar{r}_4 + b_1r_3\bar{r}_2\bar{b}_4 + g_1b_3\bar{g}_2\bar{b}_4 + g_1b_3\bar{b}_2\bar{g}_4 + b_1g_3\bar{b}_2\bar{g}_4 + b_1g_3\bar{g}_2\bar{b}_4\Big). \tag{24}$$

5. Total wave function

The total wave functions are obtained by the direct product of wave functions of orbital, spin, color, and flavor wave functions. Because we are interested in the states with quantum number $J^P = 1^-$, there must be orbital angular momentum excitation. The experiment suggests that the excited orbital angular quantum number should exist in one subcluster. So we follow the suggestion, set $l_1 = 1$, $l_2 = 0$ or $l_1 = 0$, $l_2 = 1$. It is worthwhile to mention that it is not easy to calculate matrix elements which relate to the excited orbital angular momenta of the systems. In this case, we use infinitesimally shifted Gaussian method to calculate the matrix elements.

Finally, the total wave function of the tetraquark system is written as

$$\Psi^{i,j,k}_{JM_J} = \mathcal{A}\Big[[\psi_L\chi_S^{\sigma_i}]_{JM_J}\chi_j^{fi}\chi_k^{ci}\Big], \tag{25}$$

where the $\mathcal{A}$ is the antisymmetry operator of the system which guarantees the antisymmetry of the total wave functions when identical particles exchange. Because there are no identical particles in $b\bar{b}q\bar{q}$ tetraquark system, the $\mathcal{A} = 1$. At last, we solve the following Schrödinger equation to obtain eigenenergies of the system, with the help of the Rayleigh-Ritz variational principle,

$$H\Psi^{i,j,k}_{JM_J} = E\Psi^{i,j,k}_{JM_J}, \tag{26}$$

where $\Psi^{i,j,k}_{JM_J}$ is the wave function of the four-quark states, which is the linear combinations of the above channel wave functions.

III. REAL-SCALING METHOD

The real-scaling method was first put forward by Taylor [17] to estimate the energies of long-lived metastable states of electron-atom, electron-molecule, and atom-diatom complexes. Then Jack Simons [18] adopted this method to study resonance state. The real-scaling method was firstly applied to the quark model developed by Emiko Hiyama *et al.* [19] to search for P_c state in the $qqqc\bar{c}$ system. Different from the other computing resonances method based on a stabilized eigenvector, the real-scaling

method can estimate the decay width directly from the stabilization graph.

In this approach, a factor α is used to scale the finite volume. The "false resonant states" reproduced by superabundant colorful subclusters (molecular hidden-color state or diquark-antidiquark state) will fall down to the corresponding threshold, while the genuine resonances will survive after coupling to the scattering states and keep stable with increasing α. In this way, the genuine resonances will have two forms: (a) If the energy of a scattering state is far away from that of the resonance, which means there is a weak coupling (or no coupling) between the resonances and the scattering state, the shape of the resonance is a stable straight line [see Fig. 3(a)]; (b) If the energy of a scattering state is close to the resonance, there is a strong coupling between the resonance and the scattering state, which would act as an avoid crossing structure between two declining lines [see in Fig. 3(b)]. By this means, we can estimate the decay width from the slopes of resonance and scattering states from Eq. (27), where S_r donates the slope of resonance, S_s donates the slope of scattering state, and α_c donates energy-level difference between the resonance and the scattering state. In addition, if α is increasing continually, the avoid crossing structure will repeat again

$$\Gamma = 4|V(\alpha_c)|\frac{\sqrt{|S_r||S_s|}}{|S_r - S_s|}. \tag{27}$$

IV. RESULTS AND DISCUSSIONS

In this section, we present the numerical results of our calculation. Given the possibility of the newly observed state $\Upsilon(10753)$ being a two-quark or four-quark state, we conduct a comprehensive calculation that includes both two-quark and four-quark structures. The calculation results for all mesons, from light to heavy, used in this paper are listed in Table II. Regarding the four-quark calculation, our main objective is to search for resonance states that could serve as candidates for the $\Upsilon(10753)$. As a first step, we perform a dynamic calculation based on GEM to determine whether there exists any bound state. In our calculation, we expand the wave function of two subclusters and the wave function of relative motion in the Schrödinger equation using Gaussian bases. Since the spin-orbit interaction has little effect on the $\chi_{bJ,J=0,1,2}$ meson, we initially neglect it and only consider the center force in the four-quark calculation. Thus, we classify the states according to the total spin S of the four-quark system, marking $S = 0$ with ${}^1P_1$ (${}^{2S+1}L_J$), $S = 1$ with ${}^3P_1$, and $S = 2$ with ${}^5P_1$. All four-quark systems with spin $S = 0, 1, 2$ can couple with $L = 1$ to give a total angular momentum of $J = 1$. After obtaining the energies using the generalized eigenequation, we compare the results obtained from the two sets of parameters to reduce the uncertainty in our outcome. The first set of parameters is labeled as Para.1 and the second set as Para.2 for convenience.

TABLE III. Mass, in MeV, and probabilities of the different components, in %, of the mixing Υ state, units in MeV.

Mixing State	Mass	$\mathcal{P}[\Upsilon(4S)]$	$\mathcal{P}[\Upsilon(3D)]$
$\text{Meson}_{\Upsilon(10564)}$	10564	99.9%	0.1%
Mixing State	Mass	$\mathcal{P}[\Upsilon(4S)]$	$\mathcal{P}[\Upsilon(3D)]$
$\text{Meson}_{\Upsilon(10631)}$	10631	0.1%	99.9%
Mixing State	Mass	$\mathcal{P}[\Upsilon(5S)]$	$\mathcal{P}[\Upsilon(4D)]$
$\text{Meson}_{\Upsilon(10863)}$	10863	99.9%	0.1%

A. Two-quark calculation

The Belle Collaboration observed the mass of $\Upsilon(10753)$ to be 10753 ± 6 MeV. According to the suggestions from Refs. [5,6], $\Upsilon(10753)$ may be a mixing of $\text{Meson}_{\Upsilon(4S)}$ and $\text{Meson}_{\Upsilon(3D)}$ in the quark model. To investigate this possibility, we calculated the masses and compositions of $\text{Meson}_{\Upsilon(4S)}$, $\text{Meson}_{\Upsilon(3D)}$, and $\text{Meson}_{\Upsilon(5S)}$, which are listed in Tables II and III. We found that the mass of $\text{Meson}_{\Upsilon(4S)}$ is 10.56 GeV, while the mass of $\text{Meson}_{\Upsilon(3D)}$ is 10.63 GeV. The energy of $\text{Meson}_{\Upsilon(5S)}$ is up to 10.8 GeV. Based on their masses, $\text{Meson}_{\Upsilon(4S)}$ is a more likely candidate for $\Upsilon(10580)$, while the $\text{Meson}_{\Upsilon(3D)}$ is unlikely to be a candidate for $\Upsilon(10753)$ due to its mass being about 110 MeV less than that of $\Upsilon(10753)$ in our work. Similarly, the mass difference between $\text{Meson}_{\Upsilon(4S)}$ and $\Upsilon(10753)$ makes $\text{Meson}_{\Upsilon(4S)}$ an unlikely candidate for $\Upsilon(10753)$.

Moreover, the coupling matrix element between $\text{Meson}_{\Upsilon(4S)}$ and $\text{Meson}_{\Upsilon(3D)}$ is small due to the large mass of the b quark, leading to weak S-D mixing effects of only about 0.1%. Thus, $\Upsilon(10753)$ cannot be a two-quark structure in our work, while $\Upsilon(10580)$ and $\Upsilon(10860)$ can be traditional mesons of $\text{Meson}_{\Upsilon(4S)}$ and $\text{Meson}_{\Upsilon(5S)}$, respectively. Additionally, according to the suggestion from Belle that $\Upsilon(10753)$ and $\Upsilon(10860)$ may have different substructures, we confirm that $\Upsilon(10860)$ is a two-quark substructure, while $\Upsilon(10753)$ may have a non-$q\bar{q}$ substructure.

B. Four-quark calculation

The presented results in Tables IV–VI provide a comprehensive analysis of all possible $b\bar{q}q\bar{b}$ tetraquark states with negative parity. The tables display the indices of orbit, flavor, spin, and color wave functions for each channel, as well as the energy, threshold, and binding energy for each physical channel under two sets of parameters. In the theoretical framework of multiquark systems, an essential criterion for determining the existence of resonances is the presence of attractive interactions in the physical channels.

TABLE IV. The results for system with $^{2S+1}L_J = {}^1P_1$. The "$[\text{meson}]_8$" denotes the molecular color-octet state. "$[\text{subdiquark}]^{\text{spin}}_{\text{color}}$" denotes the diquark state, and "$[\text{subantidiquark}]^{\text{spin}}_{\text{anti-color}}$" denotes the antidiquark state. The calculated eigenenergies closest to $\Upsilon(10753)$ are listed at the bottom of table, which denoted by $^{2S+1}E_J(\text{eigenenergy})$.The abbreviation "c.c.s.c" stands for "coupled-color-singlet-channels", while "c.c.e.c" stands for "coupled-color-excited-channels". (unit: MeV).

$\lvert R_i\rangle$	$\lvert F_j\rangle$	$\lvert S_k\rangle$	$\lvert C_n\rangle$	Channel	E_1	$E^{\text{Theo}}_{1\text{th}}$	E_{1B}	E_2	$E^{\text{Theo}}_{2\text{th}}$	E_{2B}	$E^{\text{Exp}}_{\text{th}}$
$i=1$	$j=1$	$k=1$	$n=1$	$B_1'B$	11105	11104	0	11113	11111	0	11005
$i=1$	$j=1$	$k=2$	$n=1$	B_JB^*	11169	11168	0	11177	11175	0	11056
$i=1$	$j=2$	$k=1$	$n=1$	$h_b\eta$	10492	10489	0	10481	10481	0	10447
$i=1$	$j=2$	$k=2$	$n=1$	$\chi_{bJ}\omega$	10685	10684	0	10684	10684	0	10675
$i=2$	$j=2$	$k=2$	$n=1$	Υb_J	10836	10834	0	10813	10813	0	10741
$i=2$	$j=2$	$k=1$	$n=1$	$\eta_b h$	10992	10990	0	10979	10979	0	10565
c.c.s.c for Para.1:					10492						
c.c.s.c for Para.2:					10481						
$i=1$	$j=1$	$k=1$	$n=2$	$[B_1']_8[B]_8$	11148	⋯	⋯	11141	⋯	⋯	⋯
$i=1$	$j=1$	$k=2$	$n=2$	$[B_J]_8[B^*]_8$	11099	⋯	⋯	11090	⋯	⋯	⋯
$i=1$	$j=2$	$k=1$	$n=2$	$[h_b]_8[\eta]_8$	11103	⋯	⋯	11115	⋯	⋯	⋯
$i=1$	$j=2$	$k=2$	$n=2$	$[\chi_{bJ}]_8[\omega]_8$	10982	⋯	⋯	10996	⋯	⋯	⋯
$i=2$	$j=2$	$k=2$	$n=2$	$[\Upsilon]_8[b_J]_8$	11342	⋯	⋯	11353	⋯	⋯	⋯
$i=2$	$j=2$	$k=1$	$n=2$	$[\eta_b]_8[h]_8$	11299	⋯	⋯	11310	⋯	⋯	⋯
$i=3$	$j=3$	$k=1$	$n=3$	$[bq]^0_3[\bar{b}\,\bar{q}]^0_{\bar{3}}$	11312	⋯	⋯	11312	⋯	⋯	⋯
$i=3$	$j=3$	$k=1$	$n=4$	$[bq]^0_6[\bar{b}\,\bar{q}]^0_{\bar{6}}$	11240	⋯	⋯	11230	⋯	⋯	⋯
$i=3$	$j=3$	$k=2$	$n=3$	$[bq]^1_3[\bar{b}\,\bar{q}]^1_{\bar{3}}$	11339	⋯	⋯	11337	⋯	⋯	⋯
$i=3$	$j=3$	$k=2$	$n=4$	$[bq]^1_6[\bar{b}\,\bar{q}]^1_{\bar{6}}$	11202	⋯	⋯	11192	⋯	⋯	⋯
c.c.e.c for Para.1:					10813	10926	10943	11047			
c.c.e.c for Para.2:					10800	10923	10950	11058			
Complete coupled-all-channels for Para.1:						10492					
Complete coupled-all-channels for Para.2:						10481					

In this study, we employ a rigorous analysis to assess the binding energy (E_B) of each color-singlet state by comparing its theoretical calculated value with its corresponding threshold value ($E - E_{\text{th}}$). The binding energy serves as an indicator of attraction within the system. It is important to note that color-excited states inherently possess internal attraction due to color interactions. For clarity, we focus on reporting the binding energy (E_B) exclusively for the color-singlet structures in Tables IV–VI, omitting the E_B values for the color-excited structures. When examining the color-singlet structures, a positive E_B value greater than zero signifies a scattering state, indicating the absence of a resonant behavior, so we manually assign a value of zero to such cases, where E_B exceeds zero. Subsequently, the real-scaling method is employed to investigate whether states exhibiting attractive interactions, including both color-excited and color-singlet states with E_B values less than zero, can indeed form resonance states.

In the $^1P_1$ configuration, we find six color-singlet channels, namely $B_1'B$, B_JB^*, $h_b\eta$, $\chi_{bJ}\omega$, Υb_J, and $\eta_b h$, as listed in Table IV. Additionally, there are six color-octet channels and six diquark-antidiquark channels in the color-excited configuration, as shown in Table IV. We observe that the energy levels of the color-singlet states in both sets of parameters range from 10.5 GeV to 11.0 GeV, with $h_b\eta$ having the lowest energy and B_JB^* having the highest. The second set of parameters shows only marginal differences in the energy levels. However, there are no bound states in either set of parameters, indicating that these are scattering states. In contrast, the energies of the color-excited states are approximately 11.0 GeV in both sets of parameters. The lowest-energy state $[\chi_{bJ}]_8[\omega]_8$ has an energy of around 10.9 GeV, while the second lowest-energy state $[B_J]_8[B^*]_8$ has an energy of around 11.9 GeV. Due to the presence of a large number of channels with similar energies, the channel coupling in the color-excited configuration is strong. As a result, the energy of $[\chi_{bJ}]_8[\omega]_8$ is reduced to around 10.8 GeV, and that of $[B_J]_8[B]_8$ is reduced to around 11.0 GeV. Interestingly, the energy of $[\chi_{bJ}]_8[\omega]_8$ after channel coupling is relatively close to the mass of the recently discovered $\Upsilon(10753)$ state, indicating that $[\chi_{bJ}]_8[\omega]_8$ may be a promising candidate for this state. Furthermore, we have conducted a coupling calculation for all physical channels in both the color-singlet and color-excited structures. We find that the lowest-energy physical channel, $h_b\eta$, is not pushed below the threshold, indicating that there are no bound states in the $^1P_1 b\bar{q}q\bar{b}$ system.

The ^3P_J tetraquark state has a total spin of 1 and can be formed by coupling the spins of two subgroups, resulting in three possible spin configurations: 0×1, 1×0, and 1×1.

TABLE V. The results for system with $^{2S+1}L_J = {}^3P_J$. The "$[\text{meson}]_8$" denotes the molecular color-octet state. "$[\text{subdiquark}]^{\text{spin}}_{\text{color}}$" denotes the diquark state, and "$[\text{subantidiquark}]^{\text{spin}}_{\text{anticolor}}$" denotes the antidiquark state. The calculated eigenenergies closest to $\Upsilon(10753)$ are listed at the bottom of table, which denoted by $^{2S+1}E_J(\text{eigenenergy})$. The abbreviation "c.c.s.c" stands for "coupled-color-singlet-channels", while "c.c.e.c" stands for "coupled-color-excited-channels". (unit: MeV).

$\lvert R_i\rangle$	$\lvert F_j\rangle$	$\lvert S_k\rangle$	$\lvert C_n\rangle$	Channel	E_1	$E^{\text{Theo}}_{1\text{th}}$	E_{1B}	E_2	$E^{\text{Theo}}_{2\text{th}}$	E_{2B}	$E^{\text{Exp}}_{\text{th}}$
$i=1$	$j=1$	$k=1$	$n=1$	$B_1'B^*$	11162	11161	0	11171	11170	0	11051
$i=1$	$j=1$	$k=2$	$n=1$	B_JB	11112	11111	0	11121	11120	0	11011
$i=1$	$j=1$	$k=3$	$n=1$	B_JB^*	11169	11168	0	11178	11177	0	11057
$i=1$	$j=2$	$k=1$	$n=1$	$h_b\omega$	10684	10682	0	10684	10683	0	10681
$i=1$	$j=2$	$k=2$	$n=1$	$\chi_{bJ}\eta$	10493	10491	0	10484	10482	0	10441
$i=1$	$j=2$	$k=3$	$n=1$	$\chi_{bJ}\omega$	10685	10684	0	10686	10684	0	10674
$i=2$	$j=2$	$k=1$	$n=1$	$\eta_b b_J$	10883	10881	0	10862	10860	0	10679
$i=2$	$j=2$	$k=2$	$n=1$	Υh	10945	10943	0	10933	10931	0	10626
$i=2$	$j=2$	$k=3$	$n=1$	Υb_J	10992	10990	0	10980	10979	0	10741
c.c.s.c for Para.1:					10493						
c.c.s.c for Para.2:					10484						
$i=1$	$j=1$	$k=1$	$n=2$	$[B_1']_8[B^*]_8$	11145	⋯	⋯	11137	⋯	⋯	⋯
$i=1$	$j=1$	$k=2$	$n=2$	$[B_J]_8[B]_8$	11148	⋯	⋯	11140	⋯	⋯	⋯
$i=1$	$j=1$	$k=3$	$n=2$	$[B_J]_8[B^*]_8$	11122	⋯	⋯	11114	⋯	⋯	⋯
$i=1$	$j=2$	$k=1$	$n=2$	$[h_b]_8[\omega]_8$	11014	⋯	⋯	11028	⋯	⋯	⋯
$i=1$	$j=2$	$k=2$	$n=2$	$[\chi_{bJ}]_8[\eta]_8$	11103	⋯	⋯	11115	⋯	⋯	⋯
$i=1$	$j=2$	$k=3$	$n=2$	$[\chi_{bJ}]_8[\omega]_8$	10998	⋯	⋯	11012	⋯	⋯	⋯
$i=2$	$j=2$	$k=1$	$n=2$	$[\eta_b]_8[b_J]_8$	11319	⋯	⋯	11331	⋯	⋯	⋯
$i=2$	$j=2$	$k=2$	$n=2$	$[\Upsilon_b]_8[h]_8$	11341	⋯	⋯	11353	⋯	⋯	⋯
$i=2$	$j=2$	$k=3$	$n=2$	$[\Upsilon]_8[b_J]_8$	11309	⋯	⋯	11320	⋯	⋯	⋯
$i=3$	$j=3$	$k=1$	$n=3$	$[bq]^0_3[\bar{b}\,\bar{q}]^1_{\bar{3}}$	11331	⋯	⋯	11331	⋯	⋯	⋯
$i=3$	$j=3$	$k=1$	$n=4$	$[bq]^0_6[\bar{b}\,\bar{q}]^1_{\bar{6}}$	11234	⋯	⋯	11223	⋯	⋯	⋯
$i=3$	$j=3$	$k=2$	$n=3$	$[bq]^1_3[\bar{b}\,\bar{q}]^0_{\bar{3}}$	11315	⋯	⋯	11315	⋯	⋯	⋯
$i=3$	$j=3$	$k=2$	$n=4$	$[bq]^1_6[\bar{b}\,\bar{q}]^0_{\bar{6}}$	11239	⋯	⋯	11228	⋯	⋯	⋯
$i=3$	$j=3$	$k=3$	$n=3$	$[bq]^1_3[\bar{b}\,\bar{q}]^1_{\bar{3}}$	11337	⋯	⋯	11336	⋯	⋯	⋯
$i=3$	$j=3$	$k=3$	$n=4$	$[bq]^1_6[\bar{b}\,\bar{q}]^1_{\bar{6}}$	11217	⋯	⋯	11207	⋯	⋯	⋯
c.c.e.c for Para.1:					10856	10893	10932	10956			
c.c.e.c for Para.2:					10846	10883	10925	10968			
Complete coupled-all-channels for Para.1:						10493					
Complete coupled-all-channels for Para.2:						10484					

Taking into account the four spatial-flavor configurations and two color wave functions, there are 24 physical channels to consider. We individually studied nine molecular color-singlet states, nine molecular hidden-color states, and six diquark-antidiquark states, as summarized in Table V. However, even with the coupling of so many physical channels, we did not find any evidence of bound states using two sets of parameters. The lowest-energy physical channel is the $\chi_{bJ}\eta$ state, with an energy of around 10,490 MeV and a binding energy of 0 MeV (as indicated by E_{1B} and E_{2B} in row 6 of the table). The molecular energy of the color-singlet state with $b\bar{q}$-$q\bar{b}$ structure is between 11,110 MeV and 11,200 MeV, while the molecular energy of the color-singlet state with $b\bar{b}$-$q\bar{q}$ structure fluctuates greatly, ranging from 10,480 MeV to 10,990 MeV. However, in the case of two spatial structures, the energy of their color excited states is relatively similar, ranging from 10,990 MeV to 10,300 MeV. The coupling effect of the many physical channels in the color-excited structure of the ^3P_J tetraquark system shows that the lowest-energy distributions in the final results are between 10,850 MeV and 10,950 MeV. Nonetheless, these states are unlikely to be the experimentally observed $\Upsilon(10753)$ due to their higher energies. Since many physical channels have energies that are similar to the energy of the color-excited states in the color-singlet channel, their channel coupling effect is significant, and they may either decay into the corresponding scattering states or depress to the level of the $\Upsilon(10753)$ state.

The ^5P_J $b\bar{q}q\bar{b}$ system consists of three color-singlet states, three hidden-color states, and two diquark-antidiquark states, all of which are scattering states. Our channel-coupling calculation of ^5P_J tetraquark states shows that there are no bound states in color-singlet meson channels. Although the

TABLE VI. The results for system with $^{2S+1}L_J = {}^5P_J$. The "$[\text{meson}]_8$" denotes the molecular color-octet state. "$[\text{subdiquark}]^{\text{spin}}_{\text{color}}$" denotes the diquark state, and "$[\text{subantidiquark}]^{\text{spin}}_{\text{anti-color}}$" denotes the antidiquark state. The calculated eigenenergies closest to $\Upsilon(10753)$ are listed at the bottom of table, which denoted by $^{2S+1}E_J(\text{eigenenergy})$.The abbreviation "c.c.s.c" stands for "coupled-color-singlet-channels", while "c.c.e.c" stands for "coupled-color-excited-channels". (unit: MeV).

$\|R_i\rangle$	$\|F_j\rangle$	$\|S_k\rangle$	$\|C_n\rangle$	Channel	E_1	$E^{\text{Theo}}_{1\text{th}}$	E_{1B}	E_2	$E^{\text{Theo}}_{2\text{th}}$	E_{2B}	$E^{\text{Exp}}_{\text{th}}$
$i=1$	$j=1$	$k=6$	$n=1$	B_JB^*	11169	11168	0	11178	11178	0	11056
$i=1$	$j=2$	$k=6$	$n=1$	$\chi_{bJ}\omega$	10685	10684	0	10686	10684	0	10675
$i=2$	$j=2$	$k=6$	$n=1$	Υb_J	10992	10990	0	10980	10979	0	10741
c.c.s.c for Para.1:					10685						
c.c.s.c for Para.2:					10686						
$i=1$	$j=1$	$k=6$	$n=2$	$[B_J]_8[B^*]_8$	11166	⋯	⋯	11159	⋯	⋯	⋯
$i=1$	$j=2$	$k=6$	$n=2$	$[\chi_{bJ}]_8[\omega]_8$	11029	⋯	⋯	11043	⋯	⋯	⋯
$i=2$	$j=2$	$k=6$	$n=2$	$[\Upsilon]_8[b_J]_8$	11328	⋯	⋯	11340	⋯	⋯	⋯
$i=3$	$j=3$	$k=6$	$n=3$	$[bq]^1_3[\bar{b}\,\bar{q}]^1_{\bar{3}}$	11332	⋯	⋯	11332	⋯	⋯	⋯
$i=3$	$j=3$	$k=6$	$n=4$	$[bq]^1_6[\bar{b}\,\bar{q}]^1_{\bar{6}}$	11247	⋯	⋯	11237	⋯	⋯	⋯
c.c.e.c for Para.1:					10935	10986	11231				
c.c.e.c for Para.2:					10927	11000	11242				
Complete coupled-all-channels for Para.1:						10685					
Complete coupled-all-channels for Para.2:						10686					

energy of the lowest channels, $[\chi_{bJ}]_8[\omega]_8$, is the same for all color-excited states in the table with $^{2S+1}L_J = {}^5P_J$, we find that the lowest energy of the channel-coupling result for these states is about 80 MeV higher than that of the color-excited state with the other $^{2S+1}L_J$. This indicates that the coupling effect plays a relatively small role in ^5P_J tetraquark states, given that the physical channel number of this system is smaller than that of $^1P_1$ $b\bar{q}q\bar{b}$ and ^3P_J $b\bar{q}q\bar{b}$ systems. Furthermore, we observe that the energies of all physical channels, including color-singlet and color-excited states, are close to or greater than 11,000 MeV, except for $\chi_{bJ}\omega$, which has an energy around 10,680 MeV for two sets of parameters. Overall, our findings suggest that ^5P_J tetraquark states are unlikely to account for the $\Upsilon(10753)$ particle observed by the Belle Collaboration, given the energy of every color-singlet channel, which are all scattering states, and the results of channel coupling of color-excited states, with the lowest energy of about 10,930 MeV being much larger than the energy of $\Upsilon(10753)$.

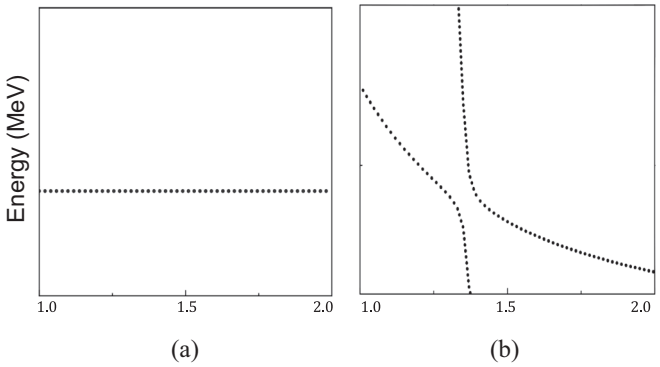

FIG. 3. Two forms of resonant states: (a) the resonance has weak coupling (or no coupling) with the scattering states; (b) the resonances has strong coupling with the scattering states.

The table shows that the energy of $[\chi_{bJ}]_8[\omega]_8$ in the color-octet structure is the lowest among all color-excited structures, and this result is consistent across all parameter sets. This is due to the fact that the attraction between bivector mesons is stronger than that between vector-scalar and scalar-scalar mesons. The interaction between scalar and vector mesons has been studied in Ref. [20], where it was found that one-gluon exchange and kinetic energy play a significant role in the meson-meson interaction. Among all color-octet states, there are three combinations of bivector mesons: $[B_J]_8[B^*]_8$, $[\chi_{bJ}]_8[\omega]_8$, and $[\Upsilon]_8[b_J]_8$. The $[\chi_{bJ}]_8[\omega]_8$ state has the lowest energy because its color-singlet state $\chi bJ\omega$ has the lowest energy. Table IV–VI presents four energy levels from the color-excited state structure that are strong candidates for the $\Upsilon(10753)$ state, with energies ranging from 10,700 MeV to 10,800 MeV. In Table IV, two energy levels, 10,813 MeV and 10,800 MeV, correspond to the same state but under different parameter sets. This state is labeled as $R(0, 10761 \pm 7)$ [where the symbol $R(\text{spin}, \text{centervalue} \pm \text{error})$ denotes the resonant state] in Fig. 4 when using the real-scaling method, with the upper limit being the value of Para.1 and the lower limit being the value of Para.2. The other two energy levels, 10856 MeV and 10846 MeV, listed in Table V are represented as $R(1, 10815 \pm 5)$ in Fig. 5. Furthermore, Figs. IV–VI illustrate five other resonances apart from the two mentioned previously: $R(0, 10895 \pm 5)$, $R(1, 10844 \pm 7)$, $R(1, 10895 \pm 5)$, $R(2, 10896 \pm 5)$, and $R(2, 10970 \pm 5)$.

Our calculations indicate that the $b\bar{b}q\bar{q}$ system does not have a limit state and that the only resonant state

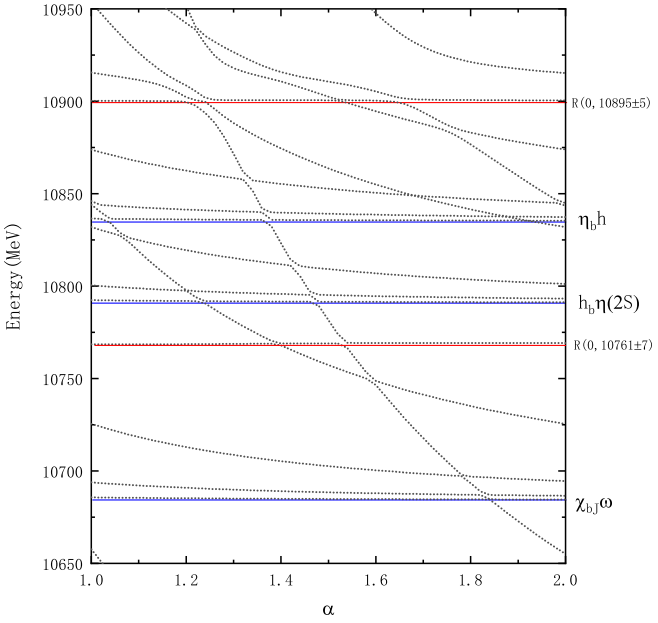

FIG. 4. Energy spectrum of $^1P_1$ states. The red line depicts the resonant state, with the upper and lower boundaries of the resonant state determined by two different sets of parameters, while the blue line represents the physical threshold.

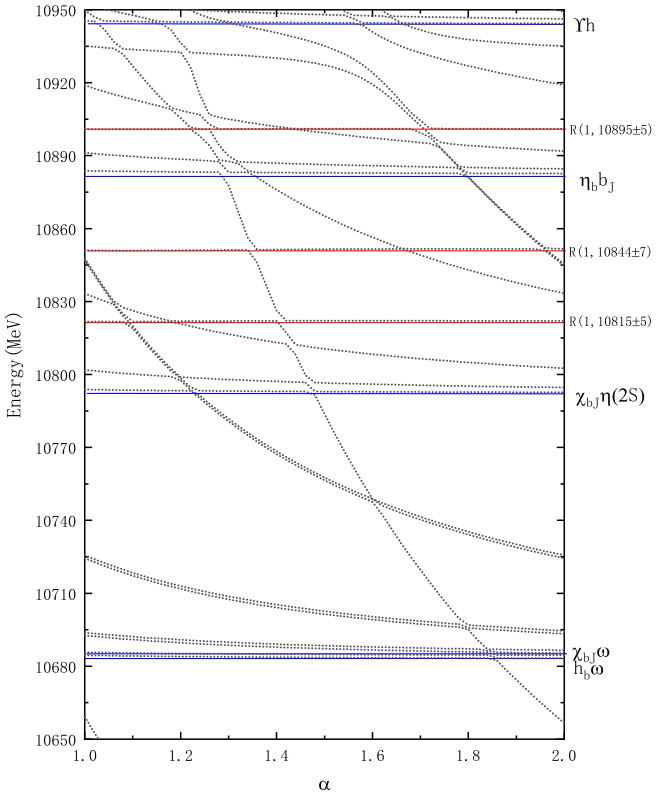

FIG. 5. Energy spectrum of ^3P_J states. The red line depicts the resonant state, with the upper and lower boundaries of the resonant state determined by two different sets of parameters, while the blue line represents the physical threshold.

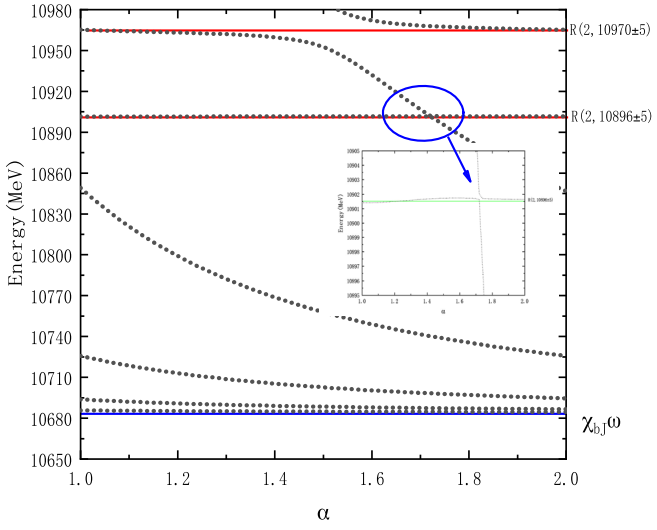

FIG. 6. Energy spectrum of ^5P_J states. The red line depicts the resonant state, with the upper and lower boundaries of the resonant state determined by two different sets of parameters, while the blue line represents the physical threshold.

that may exist is the color excited state, whose lowest energy is $[\chi_{bJ}]_8[\omega]_8$. The states with the lowest energy in Figs. 4–6 are $R(0, 10761 \pm 7)$, $R(1, 10815 \pm 5)$, and $R(2, 10896 \pm 5)$, and their primary components should all be $[\chi_{bJ}]_8[\omega]_8$ according to the channel-coupling effect. To explore the internal structure of other resonances, we calculated the root-mean-square (rms) distance between quarks of each resonant state, listed in Table IX. The rms reveals that the three resonances $R(0, 10895 \pm 5)$, $R(1, 10844 \pm 7)$, and $R(1, 10895 \pm 5)$ have a $b\bar{b}$-$q\bar{q}$ color-octet structure, with $r_{\bar{b}b}$ near 0.24 fm. In contrast, the resonant state $R(2, 10970 \pm 5)$ has $r_{b(\bar{b})-q(\bar{q})}$, $r_{q\bar{q}}$ values close to 1 fm, indicating that this state has a significant molecular component. The $b\bar{b}q\bar{q}$ structure is the primary structure of several resonances with energies between 10,750 MeV and 10,970 MeV, and their decay widths range from 1 MeV to 10 MeV (see Table VII), which are comparable. However, the resonance $R(2, 10970 \pm 5)$ has a significantly larger width of around 120 MeV due to its significant molecular component. Due to the arbitrary nature of the slope assessment of S_r and S_c, the decay

TABLE VII. The width of candidates of $\Upsilon(10753)$. Herein we use "$^{2S+1}R_J$(eigenenergy)" denotes the stable resonance with a definite spin. (unit: MeV).

State	$R(0, 10761 \pm 7)$	$R(0, 10895 \pm 5)$	
Width	10.8 ± 5.2	1.8 ± 1.7	
State	$R(1, 10815 \pm 5)$	$R(1, 10844 \pm 7)$	$R(1, 10895 \pm 5)$
Width	1.5 ± 0.3	2.7 ± 0.1	1.7 ± 1.0
State	$R(2, 10896 \pm 5)$	$R(2, 10970 \pm 5)$	
Width	0.9 ± 0.3	120.0 ± 40	

TABLE VIII. The contribution of the different potential energies of the resonant states, units in MeV.

Resonance		Q.M.	K.E.	$V_{\rm con}$	$V_{\rm oge}$	V_χ	V_s
$R(0, 10761 \pm 7)$	Parameters 1	10936	1200	151	−1606	64	23
	Parameters 2	10958	1215	144	−1651	65	25
$R(0, 10895 \pm 5)$	Parameters 1	10936	1045	190	−1272	−19	21
	Parameters 2	10958	1055	183	−1309	−19	18
$R(1, 10815 \pm 5)$	Parameters 1	10936	1110	167	−1574	61	22
	Parameters 2	10958	1122	161	−1515	61	23
$R(1, 10844 \pm 7)$	Parameters 1	10936	1129	174	−1389	−20	22
	Parameters 2	10958	1143	161	−1427	−21	33
$R(1, 10895 \pm 5)$	Parameters 1	10936	1046	191	−1275	−19	22
	Parameters 2	10958	1057	186	−1313	−19	22
$R(2, 10896 \pm 5)$	Parameters 1	10936	1046	192	−1475	−19	21
	Parameters 2	10958	1055	184	−1309	−19	21
$R(2, 10970 \pm 5)$	Parameters 1	10936	844	162	−994	−19	21
	Parameters 2	10958	882	175	−1043	−16	20

TABLE IX. The root-mean-square distance between quarks of resonant states.

Resonance	$r_{b-\bar{b}}$	$r_{b(\bar{b})-q(\bar{q})}$	$r_{q-\bar{q}}$
$R(0, 10761 \pm 7)$	0.224	0.713	0.695
$R(0, 10895 \pm 5)$	0.255	0.827	0.739
$R(1, 10815 \pm 5)$	0.239	0.800	0.710
$R(1, 10844 \pm 7)$	0.236	0.808	0.754
$R(1, 10895 \pm 5)$	0.247	0.828	0.737
$R(2, 10896 \pm 5)$	0.245	0.828	0.734
$R(2, 10970 \pm 5)$	0.680	0.832	0.920

width of $R(2, 10896 \pm 5)$ and $R(2, 10970 \pm 5)$ varies significantly. The width of these two sets of parameters is therefore calculated with a substantial calculation error, but the results are qualitatively similar. We figure out the contribution of each Hamiltonian component in each resonance state in order to investigate the impact of parameters on the results. The naked quark mass in Para.2 is larger overall than the naked quark mass in Para.1, as shown in the Table VIII, and as a result, Para.2's quark mass and kinetic energy Hamiltonians contribute more than those in Para.1's. However, the one-gluon-exchange effect increases as quark mass increases. These two impacts together cancel each other out, therefore our results are robust and reliable, as they are not overly sensitive to changes in the parameters.

V. SUMMARY

In the framework of a chiral-constituent quark model, we study systematically $J^P = 1^-$ $\Upsilon(10753)$ state. The two quark $\Upsilon(nS)$ states and four quarks $J^P = 1^-$ $b\bar{b}q\bar{q}$ are investigated with the help of Gaussian expansion method.

In the two-quark system, we notice that the mass of $\Upsilon(4S)$ is 10,564 MeV which is a good candidate of $\Upsilon(10580)$ observed by experiment while the $\Upsilon(5S)$ with an energy of 10,863 MeV is a possible candidate of experimental $\Upsilon(10860)$. We find that several authors suggested the S-D mixing may be helpful for increasing the mass of $3D$ of Υ state to be candidate of $\Upsilon(10753)$. However, in our theoretical calculation, the S-D mixing is very small. There are two reasons. Firstly, the mass of b quark is very big that the cross matrix element is small. Secondly, the mass difference between $\Upsilon(4S)$ and $\Upsilon(3D)$ is relatively large.

For the four-quark system, two different meson-meson structure $b\bar{b}$-$q\bar{q}$ and $b\bar{q}$-$q\bar{b}$, one diquark-antidiquark structure bq-$\bar{q}\,\bar{b}$, with all possible color, flavor, spin configurations are taken into account. Firstly, no bound state is found in every color-singlet physical channel, also in the all of color-singlet physical channel coupling. By means of coupling all of color-excited s states, several resonances, $R(0, 10761 \pm 7)$, $R(1, 10815 \pm 5)$, $R(0, 10895 \pm 5)$, $R(1, 10844 \pm 7)$, $R(1, 10895 \pm 5)$, $R(2, 10896 \pm 5)$, and $R(2, 10970 \pm 5)$, are achieved in $^{2S+1}L_J = {}^1P_1, {}^3P_J, {}^5P_J$ $b\bar{q}q\bar{b}$ systems. The maximum and lower boundaries of errors represent, respectively, the calculated outcomes for two sets of various parameters.The energy of $[\chi_{bJ}]_8[\omega]_8$ is the lowest among all color excited states because of the one-boson-exchange between bivector mesons. The $[\chi_{bJ}]_8[\omega]_8$ survived the coupling with the scattering states when the real-scaling approach was applied, forming the resonant states $R(0, 10761 \pm 7)$, $R(1, 10815 \pm 5)$, and $R(2, 10896 \pm 5)$. We conclude that $R(0, 10895 \pm 5)$, $R(1, 10844 \pm 7)$, and $R(1, 10895 \pm 5)$ also belong to the $b\bar{b} - q\bar{q}$ system and may be the excited state of $[\chi_{bJ}]_8[\omega]_8$ based on the fact that the spatial structure of the latter and the resonant states is quite similar. Their decay widths range from 1 MeV to 10 MeV. The decay width of $R(2, 10970 \pm 5)$ is substantially different from that of other resonant states due to the fact that the quark spacing is 0.9–1.0 fm, indicating that $R(2, 10970 \pm 5)$ contains a significant molecular component.

According to the above discussion, the newly observed state $\Upsilon(10753)$ can be described as a compact tetraquark state $R(0, 10761 \pm 7)$ in our work. As for experimental $\Upsilon(10860)$, we can not tell directly whether it's a two-quark structure or a four-quark structure based on our present work due to the lack of decay width calculation $[\Upsilon(nS)\pi^+\pi^-]$. We didn't find resonances with energies located below 10.7 GeV, which corresponds to the suggestion from Belle that no significant signal is observed for masses between 10.45 GeV and 10.65 GeV. In addition, several resonances are found with energies located in an interval 10.82–10.96 GeV, which corresponds to the suggestion from Belle that no significant signal is observed. When the spin-orbit and tensor interactions are included, all the states with $^1P_1$, ^3P_J, and ^5P_J will be mixed. Clearly, further calculation is expected.

ACKNOWLEDGMENTS

This work is supported partly by the National Natural Science Foundation of China under Grant Nos. 12205249, 11775118, and 12205125, by the Natural Science Foundation of Jiangsu Province (BK20221166), and the Funding for School-Level Research Projects of Yancheng Institute of Technology (No. xjr2022039).

[1] S. K. Choi *et al.* (Belle Collaboration), Phys. Rev. Lett. **91**, 262001 (2003).
[2] I. Adachi *et al.* (Belle-II Collaboration), Phys. Rev. Lett. **130**, 091902 (2023).
[3] A. Bondar *et al.* (Belle Collaboration), Phys. Rev. Lett. **108**, 122001 (2012).
[4] A. Garmash *et al.* (Belle Collaboration), Phys. Rev. Lett. **116**, 212001 (2016).
[5] B. Chen, A. Zhang, and J. He, Phys. Rev. D **101**, 014020 (2020).
[6] Q. Li, M. S. Liu, Q. F. Lü, L. C. Gui, and X. H. Zhong, Eur. Phys. J. C **80**, 59 (2020).
[7] Z. G. Wang, Chin. Phys. C **43**, 123102 (2019).
[8] P. Bicudo, N. Cardoso, L. Mueller, and M. Wagner, Phys. Rev. D **103**, 074507 (2021).
[9] A. Ali, L. Maiani, A. Y. Parkhomenko, and W. Wang, Phys. Lett. B **802**, 135217 (2020).
[10] Y. Yang, C. Deng, J. Ping, and T. Goldman, Phys. Rev. D **80**, 114023 (2009).
[11] J. Vijande, F. Fernandez, and A. Valcarce, J. Phys. G **31**, 481 (2005).
[12] J. Vijande and A. Valcarce, Phys. Lett. B **677**, 36 (2009).
[13] X. Hu and J. Ping, Eur. Phys. J. C **82**, 118 (2022).
[14] Y. Tan, W. Lu, and J. Ping, Eur. Phys. J. Plus **135**, 716 (2020).
[15] W. J. Deng, H. Liu, L. C. Gui, and X. H. Zhong, Phys. Rev. D **95**, 074002 (2017).
[16] E. Hiyama, Y. Kino, and M. Kamimura, Prog. Part. Nucl. Phys. **51**, 223 (2003).
[17] Howard S. Taylor, Adv. Chem. Phys. **18**, 91 (1970).
[18] J. Simons, J. Chem. Phys. **75**, 2465 (1981).
[19] E. Hiyama, A. Hosaka, M. Oka, and J. M. Richard, Phys. Rev. C **98**, 045208 (2018).
[20] Y. Wu, X. Jin, H. Huang, J. Ping, and X. Zhu, Phys. Rev. C **106**, 025204 (2022).